



**HAL**  
open science

# A comparison of a one-dimensional finite element method and the transfer matrix method for the computation of wind music instrument impedance

Robin Tournemenne, Juliette Chabassier

► **To cite this version:**

Robin Tournemenne, Juliette Chabassier. A comparison of a one-dimensional finite element method and the transfer matrix method for the computation of wind music instrument impedance. *Acta Acustica united with Acustica*, 2019, 105 (5), pp.838. 10.3813/AAA.919364 . hal-01963674v2

**HAL Id: hal-01963674**

**<https://inria.hal.science/hal-01963674v2>**

Submitted on 24 Oct 2019

**HAL** is a multi-disciplinary open access archive for the deposit and dissemination of scientific research documents, whether they are published or not. The documents may come from teaching and research institutions in France or abroad, or from public or private research centers.

L'archive ouverte pluridisciplinaire **HAL**, est destinée au dépôt et à la diffusion de documents scientifiques de niveau recherche, publiés ou non, émanant des établissements d'enseignement et de recherche français ou étrangers, des laboratoires publics ou privés.

# A comparison of a one-dimensional finite element method and the transfer matrix method for the computation of wind music instrument impedance

Robin Tournemenne<sup>1)</sup>, Juliette Chabassier<sup>1)</sup>

<sup>1)</sup> Magique 3D Team, Inria Bordeaux Sud Ouest, 200 avenue de la vieille tour, 33405 Talence Cedex, France, [firstname.lastname@inria.fr](mailto:firstname.lastname@inria.fr)

## 1 Summary

This work presents a computation tool for the calculation of wind instrument input impedance in the context of linear planar wave propagation with visco-thermal losses. The originality of the approach lies in the usage of a specific **and simple 1D** finite element method (FEM). The popular Transfer Matrix Method (TMM) is also recalled and a seamless formulation is proposed which unifies the cases cylinders vs. cones. **Visco-thermal losses, which are natural dissipation in the system, are not exactly taken into account by this method when arbitrary shapes are considered. The introduction of an equivalent radius leads to an approximation that we quantify using the FEM method. The equation actually solved by the TMM in this case is exhibited. The accuracy of the two methods (FEM and TMM) and the associated computation times are assessed and compared.** Although the TMM is more efficient in lossless cases and for lossy cylinders, the FEM is shown to be more efficient when targeting a specific precision in the realistic case of a lossy trumpet. **Some additional features also exhibit the robustness and flexibility of the FEM over the TMM.** All the results of this article are computed using the open-source python toolbox OpenWind.

## 1 Introduction

The input impedance of wind instruments is defined as its frequency dependent linear response to an input excitation. This physical quantity is of considerable advantage in understanding the instrument's playing quality, and eventually its musical behavior [Campbell(2004), Chaigne and Kergomard(2016)]. The impedance is used for various purposes, such as the analysis of the instrument's playing properties, the synthesis of their sounds and the design of their shape. Indeed, many studies try to correlate the impedance features to the instrument actual intonation, stability, tone [Backus(1976), Braden et al.(2009), Campbell(2004)]. Many syn-

thesis methods rely on the input impedance knowledge to produce realistic sounds [Silva et al.(2014)], in order to assess the quality of the physical model, or to provide musicians with virtual instruments. Wind instrument design is the goal of many current initiatives, which try to either reconstruct bores, solve inverse problems based on their measured input impedance [Kausel(2001)], improve existing instruments [Tournemenne et al.(2017)] or even develop new instruments [Buys et al.(2017)] to fulfill the aspirations of musicians.

On the one hand, since the pioneering work of Webster [Webster(1947)], many methods can measure the input impedance with varying precision and frequency range [Le Roux et al.(2008), Caussé et al.(1984), Sharp et al.(2011)]. On the other hand, physical models associated with computation methods can be used to calculate the input impedance. The current reference computation method is the transfer matrix method (TMM), which has been used in the context of wind instruments for more than 40 years [Plitnik and Strong(1979), Mapes-Riordan(1993)]. The underlying physical model can assume plane or spherical wave propagation in the pipe, mono or multi-modal propagation, viscothermal losses at the pipe walls and a radiation impedance at the pipe output, etc.

The objective of this paper is to propose a new method for the computation of the input impedance, which could noticeably facilitate and broaden numerical instrument design approaches. It is not our purpose in this article to discuss the physical model and especially the validity of the underlying physical assumptions. Although this topic is of great interest, and must rely on precise simulation / measurement comparisons, the present work only focuses on technical aspects of the impedance computation. The methodology is here presented in the simplest possible realistic acoustical case, but the present article will serve as a basis to consider more general physical models in the future. We will present a new computation approach based on a one-dimensional finite element method used on the Telegraph equations with viscothermal losses. No-

85 tice first that, compared to the TMM, the proposed  
 86 approach is therefore simply another way of solv-  
 87 ing the same equations. Notice also that the objec-  
 88 tive is not to solve the acoustical equations in 3D  
 89 [Lefebvre and Scavone(2012)], nor the Navier-Stokes  
 90 equations in 3D [Giordano(2014)]. The method pro-  
 91 posed in this paper is close to finite difference methods  
 92 [Bilbao(2009), van den Doel and Ascher(2008)], even  
 93 if it is used here in the time-harmonic context.

94 This article goes in pair with an open-source  
 95 Python 3 toolbox, Openwind [OpenWIND], that can  
 96 be freely downloaded and used to undertake numerical  
 97 experiments. After introducing the physical context  
 98 in Section 2, the practical aspects of this numerical  
 99 method (FEM) are first covered in Section 3, then  
 100 the current reference method, the Transfer Matrix  
 101 Method, is presented and its limits considering visco-  
 102 thermal losses are exhibited in Section 4. A thorough  
 103 validation is made in order to assess the precision  
 104 and performance brought by this one-dimensional fi-  
 105 nite element implementation in Section 5. The TMM  
 106 can only approximate the solution when visco-thermal  
 107 losses are considered for arbitrary shapes. We study  
 108 the related error using the introduced FEM in Section  
 109 6. Finally, computation times and several useful fea-  
 110 tures of the FEM are presented (Section 6.3) before  
 111 concluding.

## 112 2 Physics-based model

113 Consider an axisymmetric pipe occupying a domain  
 114  $\Omega \subset \mathbb{R}^3 = (Ox, Oy, Oz)$  of slowly varying cross section  
 115  $S$  and rigid walls developing along the  $x$  axis, filled  
 with air, see Figure 1.

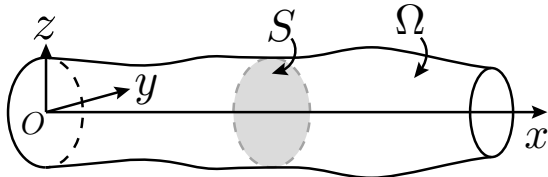


Figure 1: Definition of the space variables.  $S$  is the slowly varying section of the axisymmetric pipe.

116 The acoustic pressure  $p(x, y, z, t)$  and the three-  
 117 dimensional flow  $u(x, y, z, t)$  can be considered as  
 118 the solution to Navier-Stokes three-dimensional  
 119 equations which induce an undue computa-  
 120 tional burden in the context where only the  
 121 wave propagating phenomena are of interest.  
 122 Following the simplifications of Kirchhoff's the-  
 123 ory regarding visco-thermal losses near the pipe  
 124 walls [Kirchhoff(1868), Zwikker and Kosten(1949),  
 125 Chaigne and Kergomard(2016)], the pressure can be  
 126 considered as constant in the sections orthogonal  
 127 to the  $x$ -axis, the orthogonal components of the  
 128

Sound velocity: $c = 331.45\sqrt{T/T_0}$ m s <sup>-1</sup>
Density: $\rho = 1.2929 T_0/T$ kg m <sup>-3</sup>
Viscosity: $\mu = 1.708 e - 5(1 + 0.0029 t)$ kg m <sup>-1</sup> s <sup>-1</sup>
Thermal conductivity: $\kappa = 5.77 e - 3(1 + 0.0033 t)$ Cal/(ms °C)
Spec. heat with constant p.: $C_p = 240$ Cal/(kg °C)
Ratio of specific heats: $\gamma = 1.402$

Table 1: Numerical values [Chaigne and Kergomard(2016)] of air constants used in the model.  $t$  is the temperature in Celsius, and  $T$  the absolute temperature with  $T_0 = 273.15$ K.

three-dimensional flow can be neglected in the equa-  
 tions while the axial component can be considered  
 as axisymmetric with an analytic expression of its  
 radial dependency. Finally, we seek in the frequency  
 domain  $\hat{p}(x, \omega)$  the acoustic pressure<sup>1</sup> and  $\hat{u}(x, \omega)$  the  
 volume flow, such that the one-dimensional interior  
 equations read, for all position  $x \in [0, L]$  and angular  
 frequency  $\omega \in [\omega_{\min}, \omega_{\max}]$ ,

$$\begin{cases} Z_v(\omega, x) \hat{u} + \frac{d\hat{p}}{dx} = 0, & (1a) \\ Y_t(\omega, x) \hat{p} + \frac{d\hat{u}}{dx} = 0, & (1b) \end{cases}$$

$$(2) \begin{cases} Z_v(\omega, x) = \frac{j\omega\rho}{S(x)} [1 - \mathcal{J}(k_v(\omega)R(x))]^{-1}, \\ Y_t(\omega, x) = \frac{j\omega S(x)}{\rho c^2} [1 + (\gamma - 1)\mathcal{J}(k_t(\omega)R(x))], \end{cases}$$

$$k_v(\omega) = \sqrt{j\omega\frac{\rho}{\mu}}, \quad k_t(\omega) = \sqrt{j\omega\rho\frac{C_p}{\kappa}},$$

where  $R$  is the section radius,  $S = \pi R^2$  is the section  
 area, Table 1 describes the air constants, and we in-  
 troduce the function  $\mathcal{J}$  of a complex variable, which  
 models the dissipative terms, as

$$\mathcal{J}(z) = \frac{2 J_1(z)}{z J_0(z)}, \quad \forall z \in \mathbb{C}, \quad (3)$$

where  $J_0$  and  $J_1$  are the Bessel functions of the first  
 kind. The subscripts  $v$  and  $t$  respectively stand for  
 viscous and thermal dissipative phenomena.

Furthermore, if the dissipative terms are neglected  
 ( $\mathcal{J}$  function set to zero in the equations), the classical  
 horn equations describing plane wave propagation in  
 an axisymmetric lossless pipe can be retrieved from  
 an asymptotic analysis from Euler's equations in a  
 pipe with a slowly varying section [Rienstra(2005)].  
 For convenience, we will use the names lossy model  
 for system (1), and lossless model when  $\mathcal{J}$  is set to  
 zero in system (1).

Two boundary conditions complete the  
 problem: at the bell  $x = L$ , we im-  
 pose a radiation impedance condition

<sup>1</sup>variables with a hat ( $\hat{\cdot}$ ) denote the time-domain Fourier transform of the unknown

[Rabiner and Schafer(1978), Dalmont et al.(2001), Chaigne and Kergomard(2016)]:

$$\frac{\hat{p}(L, \omega)}{\hat{u}(L, \omega)} = Z_R(\omega), \quad (4)$$

and at the input of the pipe, we impose  $\hat{u}(0, \omega) = \lambda(\omega)$ , where  $\lambda(\omega)$  will be a source term for the system. Since all the considered equations are linear, we can consider without loss of generality  $\lambda(\omega) \equiv 1$ . In this article, we are interested in computing the input impedance

$$Z(\omega) := \frac{\hat{p}(0, \omega)}{\hat{u}(0, \omega)} = \hat{p}(0, \omega). \quad (5)$$

Finally, the considered problem is the following: compute

$$Z(\omega) = \hat{p}(0, \omega), \quad \text{where} \quad (6)$$

$$\begin{cases} \left\{ \begin{array}{l} Z_v(\omega, x) \hat{u} + \frac{d\hat{p}}{dx} = 0, \\ Y_t(\omega, x) \hat{p} + \frac{d\hat{u}}{dx} = 0, \end{array} \right. & \forall x \in [0, L] \end{cases} \quad (7a)$$

$$\hat{u}(0, \omega) = 1, \quad (7b)$$

$$\begin{cases} \frac{\hat{p}(L, \omega)}{\hat{u}(L, \omega)} = Z_R(\omega). \end{cases} \quad (7c)$$

In the subsequent sections, we are interested in possible methods to solve system (7). We will first present the Finite Element Method and then the Transfer Matrix Method.

### 3 Finite element method

The finite element method (FEM) relies on a variational formulation of the entire system in usual infinite dimensional Sobolev spaces [Brezis(2011)], followed by the definition of finite dimensional spaces in which we seek numerically the solution. Recall that the Sobolev spaces  $L^2$  and  $H^1$  can be physically interpreted as  $f \in L^2([0, L])$  if  $f$  is squared integrable on  $[0, L]$  and  $f \in H^1([0, L])$  if its gradient is squared integrable. For first order formulations as the one of system (7) (flow / pressure), the theory [Courant and Hilbert(1965), Cohen (2000)] points towards the possible following framework. Find  $\hat{p}_h \in V_h \subset H^1([0, L])$ ,  $\hat{u}_h \in W_h \subset L^2([0, L])$ , such that for all  $q_h \in V_h$ ,  $w_h \in W_h$ ,

$$\left\{ \begin{array}{l} \int_0^L \frac{j\omega\rho}{S} [1 - \mathcal{J}(k_v(\omega)R)]^{-1} \hat{u}_h \overline{w_h} + \int_0^L \frac{d\hat{p}_h}{dx} \overline{w_h} = 0 \end{array} \right. \quad (8a)$$

$$\left\{ \begin{array}{l} \int_0^L \frac{j\omega S}{\rho c^2} [1 + (\gamma - 1)\mathcal{J}(k_t(\omega)R)] \hat{p}_h \overline{q_h} - \int_0^L \frac{d\overline{q_h}}{dx} \hat{u}_h - \overline{q_h}(0)\lambda(\omega) + \frac{1}{Z_R(\omega)} \hat{p}_h(L) \overline{q_h}(L) = 0 \end{array} \right. \quad (8b)$$

where by-parts integrations of Equations (7a) have been performed, followed by the use of the boundary conditions to weakly give a value to  $\hat{u}_h(0)$  and  $\hat{u}_h(L)$ . The complex conjugate of  $z$  is noted  $\bar{z}$ . Note that other choices of by-part integrations are possible, associated with other choices of functional spaces. The type of boundary conditions and source regularity usually guide this choice. In practice, we have chosen to use standard Lagrange finite elements, hence to define the spaces  $V_h$  and  $W_h$  as follows. Other choices are possible and impact the properties of the method.

The instrument is discretized into  $N$  elements  $\{K_j\}_j$ , delimited by  $N + 1$  nodes that constitute the mesh. On each element  $K_j$  we consider  $r + 1$  interior degrees of freedom called  $\{\xi_{j,p}\}_{1 \leq p \leq r+1}$ .

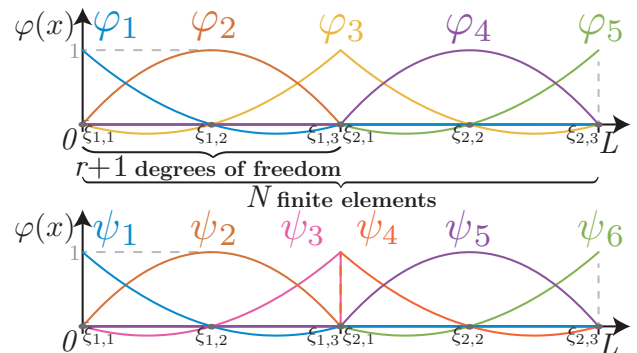


Figure 2: Basis functions with respect to  $x$  on a 2-elements mesh of  $[0, L]$ . Top : second order basis function  $\{\varphi_i\}_{1 \leq i \leq 5}$  of  $V_h$ . Bottom : second order basis function  $\{\psi_i\}_{1 \leq i \leq 6}$  of  $W_h$ . (colors online)

The finite dimensional spaces  $V_h$  and  $W_h$  are spanned by the nodal bases  $\{\varphi_i\}_{1 \leq i \leq N_{H^1}}$  and  $\{\psi_j\}_{1 \leq j \leq N_{L^2}}$  of piecewise polynomial functions of degree  $r$  (see an example of order 2 in Figure 2), which defines the order of the FEM. Consequently, the numerical solutions representing the pressure  $\hat{p}_h$  and volume flow  $\hat{u}_h$  are linear combinations of the basis functions  $\{\varphi_i\}_{1 \leq i \leq N_{H^1}}$  and  $\{\psi_j\}_{1 \leq j \leq N_{L^2}}$  respectively. In some communities, the basis functions are called shape functions. They are interpolation Lagrange polynomials (drawn Figure 2) associated to the concatenation of all the degrees of freedom of all the elements, where the nodes separating two elements are duplicated for  $W_h$  but not for  $V_h$ . Consequently, the basis functions of  $V_h$  are continuous while the ones of  $W_h$  present a discontinuity at the edges of the elements. This follows the conformal nature of the approximation, namely  $V_h \subset H^1([0, L])$  and  $W_h \subset L^2([0, L])$ . Moreover,  $N_{H^1} < N_{L^2}$  as soon as the mesh is composed of more than two elements. Finally, the integral terms in Equations (8) are evaluated through a quadrature procedure [Quarteroni et al.(2007)]. Although a high order quadrature formula could be employed to ensure exact integration, we have chosen to follow the condensation procedure (also named mass-

208 **lumping procedure**) of spectral high order finite ele-  
 209 ments [Cohen(2004)]<sup>2</sup>. **This technique is divided into**  
 210 **two joint steps: using the same points for the quadra-**  
 211 **ture and the interpolation which leads to a diagonal**  
 212 **mass matrix (condensation), and choosing as inter-**  
 213 **polation points the Gauss-Lobatto points which pre-**  
 214 **vents accuracy loss of the condensation method and**  
 215 **improves the global matrix conditioning.** Approximate  
 216 integrals that come from this procedure will be  
 217 denoted  $f$ .

Since system (8) stands for every  $w_h \in W_h$  and  $q_h \in V_h$ , it is equivalent to state that it stands for every basis vector of  $W_h$  and  $V_h$ . Besides, we abusively still denote  $\hat{u}_h$  (resp.  $\hat{p}_h$ ) for the coordinates of  $\hat{u}_h$  (resp.  $\hat{p}_h$ ) in the basis  $\{\varphi_i\}_{1 \leq i \leq N_{H^1}}$  (resp.  $\{\psi_j\}_{1 \leq j \leq N_{L^2}}$ ). Consequently, the discrete formulation equivalently takes the matrix form

$$\begin{cases} j\omega M_h^{L^2} \hat{u}_h + j\omega N_h^{L^2}(\omega) \hat{u}_h - B_h \hat{p}_h = 0 & (9a) \\ j\omega M_h^{H^1} \hat{p}_h + j\omega N_h^{H^1}(\omega) \hat{p}_h + \frac{1}{Z_R(\omega)} \Sigma_h \hat{p}_h \\ \quad + B_h^* \hat{u}_h - E_h = 0 & (9b) \end{cases}$$

where \* designates the adjoint and

$$\begin{aligned} (M_h^{L^2})_{i,j} &= \int_0^L \frac{\rho}{S} \psi_i \psi_j, & (M_h^{H^1})_{i,j} &= \int_0^L \frac{S}{\rho c^2} \varphi_i \varphi_j, \\ (N_h^{L^2})_{i,j}(\omega) &= \int_0^L \frac{\rho}{S} \frac{\mathcal{J}(k_v(\omega)R)}{1 - \mathcal{J}(k_v(\omega)R)} \psi_i \psi_j, \\ (N_h^{H^1})_{i,j}(\omega) &= \int_0^L \frac{S}{\rho c^2} (\gamma - 1) \mathcal{J}(k_t(\omega)R) \varphi_i \varphi_j, \\ (B_h)_{i,j} &= - \int_0^L \psi_i \frac{d\varphi_j}{dx}, & (E_h)_i &= \varphi_i(0), \\ (\Sigma_h)_{i,j} &= \varphi_i(L) \varphi_j(L) \end{aligned}$$

Notice that  $M_h^{L^2}$ ,  $M_h^{H^1}$ ,  $N_h^{L^2}(\omega)$ ,  $N_h^{H^1}(\omega)$  and  $\Sigma_h$  are diagonal matrices,  $B_h$  is block diagonal **where the blocks are full and of size  $r \times r + 1$**  and  $E_h$  is a vector with only one non zero entry. This discrete formulation defines the following linear system on the global unknown  $U_h$ :

$$\begin{aligned} A_h(\omega)U_h(\omega) &= L_h, & A_h(\omega) &= \begin{pmatrix} A_{11}(\omega) & A_{12}(\omega) \\ A_{21}(\omega) & A_{22}(\omega) \end{pmatrix}, \\ L_h &= \begin{pmatrix} 0 \\ E_h \end{pmatrix}, & U_h(\omega) &= \begin{pmatrix} \hat{u}_h \\ \hat{p}_h \end{pmatrix}(\omega) \end{aligned} \quad (10)$$

$$\begin{aligned} A_{11}(\omega) &= j\omega M_h^{L^2} + j\omega N_h^{L^2}(\omega) \\ A_{12}(\omega) &= -B_h, & A_{21}(\omega) &= B_h^* \\ A_{22}(\omega) &= j\omega M_h^{H^1} + j\omega N_h^{H^1}(\omega) + \frac{1}{Z_R(\omega)} \Sigma_h \end{aligned}$$

Notice that the matrix  $A_h$  is sparse and can therefore be inverted by using efficient sparse routines

<sup>2</sup>section 11.1.1 pp. 169 to 177

[scipySparse]<sup>3</sup>. Once this system is numerically solved, for a discrete set of values  $\{\omega_i\}_{1 \leq i \leq N_\omega} \in [\omega_{min}, \omega_{max}]$ , the input impedance is

$$\forall 1 \leq i \leq N_\omega, \quad Z_{FEM}(\omega_i) = L_h^* U_h(\omega_i), \quad (11)$$

which is the  $(N_{L^2} + 1)$ th term of the vector  $U_h(\omega_i)$ .

It is possible to diminish the computational burden by performing some pre-computations based on the pipe geometry and propagation hypotheses, and by taking advantage of the geometrical and arithmetical structure of the matrix  $A_h$  and of the required output [Amestoy et al.(2000)], but this is out of the scope of the current article.

Finally, for a given frequency, the  $N_{L^2}$  first terms of  $U_h$  give an approximation of the velocity at every degree of freedom along the bore, while the  $N_{H^1}$  last terms give an approximation of the pressure.

The FEM presented in this paper is implemented in OpenWind [OpenWIND], an open source (GPLv3) Python 3 toolbox.

## 4 Transfer matrix method

The transfer matrix method (TMM) consists in writing relations between output and input acoustic variables of simple geometries (cylinders, cones, Bessel and exponential bores...) from the use of the propagation equations [Caussé et al.(1984), Plitnik and Strong(1979)]. Consequently, given a radiation impedance  $Z_R(\omega)$  and discretizing the bore profile in a series of  $N_p$  parts, it is possible to compute the instrument's input impedance. Let  $\{x_i\}_{0 \leq i \leq N_p}$  be the list of positions on the bore's axis defining all the parts (with  $x_0 = 0$  and  $x_{N_p} = L$ ). We also define  $\hat{p}_i(\omega)$  and  $\hat{u}_i(\omega)$  as approximations of the pressure and the volume flow calculated by the TMM at the positions  $x_i$ . When the TMM is exact,  $\hat{p}_i(\omega) = \hat{p}(x_i, \omega)$  and  $\hat{u}_i(\omega) = \hat{u}(x_i, \omega)$ .

Formally, the relation between the input and the output of one part can be expressed as a  $2 \times 2$  matrix  $T_{i+1}(\omega)$ :

$$\begin{pmatrix} \hat{p}_i(\omega) \\ \hat{u}_i(\omega) \end{pmatrix} = \begin{pmatrix} a_{i+1}(\omega) & b_{i+1}(\omega) \\ c_{i+1}(\omega) & d_{i+1}(\omega) \end{pmatrix} \begin{pmatrix} \hat{p}_{i+1}(\omega) \\ \hat{u}_{i+1}(\omega) \end{pmatrix} \quad (12)$$

$$= T_{i+1} \begin{pmatrix} \hat{p}_{i+1}(\omega) \\ \hat{u}_{i+1}(\omega) \end{pmatrix}. \quad (13)$$

We then deduce the relation between the input and the output of the pipe:

$$\zeta = \begin{pmatrix} \hat{p}_0(\omega)/\hat{u}_L(\omega) \\ \hat{u}_0(\omega)/\hat{u}_L(\omega) \end{pmatrix} = \prod_{i=1}^{N_p} T_i(\omega) \begin{pmatrix} Z_R(\omega) \\ 1 \end{pmatrix}. \quad (14)$$

<sup>3</sup>more precisely, `scipy` is linked to a BLAS (Basic Linear Algebra Subprogram) which depends on your operating system and what has been installed on the computer. All the results of this article have been computed using the BLAS/LAPACK intel MKL 2018 and the linear system resolutions use a SuperLU procedure.



where  $\hat{u}_L(\omega)$  is the volume flow at the pipe end, and finally  $Z_{\text{TMM}} = \frac{\zeta(1)}{\zeta(2)}$ . The global transfer matrix is defined as the product of all the elementary matrices  $T_i$ . An implicit transmission condition is therefore assumed, which is the continuity of the variables between all parts. In practice, the computation is done only for a discrete set of pulsations  $\{\omega_j\}_{1 \leq j \leq N_\omega}$ . In the sequel, we will only consider the TMM for cylinders and cones. Transfer matrices for other geometries are available in the literature [Braden(2007), Chaigne and Kergomard(2016), Helie(2013)].

For the lossless propagation case, the equations can be solved analytically for cones and cylinders and therefore the TMM provides the exact input impedance. In the presence of viscothermal losses, **the dissipation terms depend non linearly on the bore radius**, see Equation (2). It turns out that exact matrices can only be derived for the cylinder and not for more complex parts for which the radius depends on the space variable ( $\hat{p}_i(\omega) \neq \hat{p}(x_i, \omega)$ ). A first empirical approach handles this difficulty for conical parts by approximating them as a succession of cylinders of increasing or decreasing radii [Caussé et al.(1984)]. A second empirical approach proposes to discretize each conical part in  $N_{\text{sub}}$  smaller cone subdivisions, and to use on each subdivision the transfer matrix derived for the cone considering lossless propagation, replacing some parameters by their lossy counterparts [Chabassier and Tournemene(2019)] evaluated at a chosen intermediate radius  $R^\odot$  [Mapes-Riordan(1993), Braden(2007)]. For a bore initially made of  $N_p$  conical parts, the total number of actual transfer matrices to compute would be  $N_{\text{TMM}} = N_p \times N_{\text{sub}}$ .

Since the viscothermal losses depend non-linearly on the radius, no optimal value for  $R^\odot$  can be immediately derived. Possible choices are the average radius  $R^\odot = (R_i + R_{i+1})/2$  [Mapes-Riordan(1993)] (where  $R_i$  and  $R_{i+1}$  are the input and output radii of the cone subdivision), or any other weighted average [Chaigne and Kergomard(2016), Helie(2013)]. In this article, we choose  $R^\odot = (2 \min(R_i, R_{i+1}) + \max(R_i, R_{i+1}))/3$ , which seems to be used in some existing implementations of the TMM.

We show (see [Chabassier and Tournemene(2019)] for more details) that using the TMM with the approximate matrix obtained with this strategy corresponds to actually solving analytically, **for the approximated solutions  $\hat{u}$  and  $\hat{p}$** , the following system of equations:

$$Z_{\text{TMM}}(\omega) = \hat{p}(0, \omega), \text{ where } \forall i \in [1, N_{\text{TMM}}], \quad (15)$$

$$\left\{ \begin{array}{l} \left\{ \begin{array}{l} Z_v^i \hat{u} + \frac{d\hat{p}}{dx} = 0, \\ Y_t^i \hat{p} + \frac{d\hat{u}}{dx} = 0, \end{array} \right. \quad \forall x \in [x_i, x_{i+1}] \quad (16a) \\ \\ Z_v^i = \frac{j\omega \rho}{S} [1 - \mathcal{J}(k_v(\omega)R_i^\odot)]^{-1}, \quad (16b) \\ Y_t^i = \frac{j\omega S}{\rho c^2} [1 + (\gamma - 1)\mathcal{J}(k_t(\omega)R_i^\odot)], \quad (16c) \\ \hat{p}(x_{i-}) = \hat{p}(x_{i+}), \quad \hat{u}(x_{i-}) = \hat{u}(x_{i+}), \quad (16d) \\ R_i^\odot = (2 \min(R(x_i), R(x_{i+1})) + \max(R(x_i), R(x_{i+1}))) / 3, \quad (16e) \\ \hat{u}(0, \omega) = 1, \quad (16f) \\ \frac{\hat{p}(L, \omega)}{\hat{u}(L, \omega)} = Z_R(\omega). \quad (16g) \end{array} \right.$$

This problem is different from the continuous problem (7) solved with the FEM. The difference lies in the approximation  $R^\odot$  inside the function  $\mathcal{J}$  for every interval  $[x_i, x_{i+1}]$  and amounts to approximating the original equation coefficients with discontinuous ones.

**Finally, we propose a formulation unifying the transfer matrices of the cylinder and the cone, which coincides in either cases to the ones of the literature [Mapes-Riordan(1993)], under visco-thermal losses.** It reads:

$$a_{i+1}(\omega) = a, \quad b_{i+1}(\omega) = b, \quad c_{i+1}(\omega) = c, \quad d_{i+1}(\omega) = d,$$

where

$$(17) \left\{ \begin{array}{l} a = \frac{R_{i+1}}{R_i} \cosh \Gamma \ell - \frac{\beta}{\Gamma} \sinh \Gamma \ell \\ b = \frac{R_i}{R_{i+1}} Z_c \sinh \Gamma \ell \\ c = \frac{1}{Z_c} \left[ \left( \frac{R_{i+1}}{R_i} - \frac{\beta^2}{\Gamma^2} \right) \sinh \Gamma \ell + \frac{\beta^2 \ell}{\Gamma} \cosh \Gamma \ell \right] \\ d = \frac{R_i}{R_{i+1}} \left( \cosh \Gamma \ell + \frac{\beta}{\Gamma} \sinh \Gamma \ell \right) \end{array} \right.$$

where

$$\Gamma \equiv \Gamma(\omega, R^\odot) = \frac{j\omega}{c} \sqrt{\frac{1 + (\gamma - 1)\mathcal{J}(k_t(\omega)R_i^\odot)}{1 - \mathcal{J}(k_v(\omega)R_i^\odot)}},$$

$$Z_c \equiv Z_c(\omega, R^\odot) = \frac{\rho c}{S(x_i)} \sqrt{\frac{[1 + (\gamma - 1)\mathcal{J}(k_t(\omega)R_i^\odot)]^{-1}}{1 - \mathcal{J}(k_v(\omega)R_i^\odot)}}$$

and

$$\beta = \frac{R_{i+1} - R_i}{\ell R_i}, \quad (18)$$

where  $R_i$  and  $R_{i+1}$  are respectively the input and output radii of the interval,  $\ell$  is the axial length of the interval, and  $R^\odot$  the previously defined quantity.

The transfer matrices for cylinders and cones in the lossless case can be similarly unified, it only requires to replace  $\Gamma$  by  $j\omega/c$  and  $Z_c$  by  $\rho c/S$ .

The TMM presented in this paper is implemented in OpenWind [OpenWind].

## 5 Validation

Unless otherwise stated, all input impedances presented hereafter are numerically computed from 20 to 2000 Hz with a 1Hz step, the temperature is set to 25 °C, and we consider a **terminal** impedance that models radiation from an infinite plane baffle [Rabiner and Schafer(1978)]:

$$Z_R(\omega) = \frac{\rho c}{S(L)} \frac{j\omega}{\alpha + j\omega\beta}, \quad (19)$$

where  $\alpha = 3c\pi/(8R)$  and  $\beta = 9\pi^2/128$ . Other flanges can be modelled with this impedance form, by adjusting consequently the coefficients  $\alpha$  and  $\beta$ , with a corresponding frequency validity range. Any other choice of radiation impedance can be done, including experimental ones, provided that the associated system of equations is well posed, meaning that its real part must be non-negative [Chandler-Wilde(1997)]. The discussion about radiation impedances is out of the scope of this paper, but it is important to note that the following conclusions regarding convergence rates and accuracy do not depend on this choice.

In the following, the FEM meshes are constructed as follows. A target element size (TES) is chosen by the user. The instrument being described by a series of radii at different axial points, some of the instrument parts might be shorter than the TES, and some might be longer. The instrument parts longer than the TES are equally divided to only obtain elements smaller or equal to the TES. **The instrument parts shorter than the TES are described by only one element having the same size than the part.** For realistic instruments, any TES choice will produce a non-uniform mesh since the instrument parts are not necessarily commensurate. The ratio  $\tau$  between the largest and smallest elements in a mesh is an indicator of this uniformity, and is equal to 1 for a uniform mesh.

Up to 8 geometries are studied in the following. One 20 cm cylinder with 5 mm radius (roughly corresponding to a trumpet leadpipe) is used to assess an error estimator for the lossy model. We use 5 different cones and one arbitrary simple discontinuous geometry to help analyze the TMM error for the lossy model. **These geometries share their dimensions with existing instruments or instruments parts. They are intentionally simple and have been selected in order to be highly sensible to visco-thermal losses (small radius or fast slope). Besides, a trumpet-like bore based on measurements of a real commercial trumpet is used to provide a realistic study of the lossless and lossy models.** Its bore is made of 9 cones to describe the mouthpiece, 4 cones for the leadpipe, 1 central cylinder and 20 cones for the bell (33 cones in total). Apart from the cylinder, the 7 other geometries are described in Figure 3. Notice that the 3 cones corresponding to the mouthpiece cup, backbore, and

the trumpet leadpipe parts would normally be inside the instrument and yet we consider here their input impedance with open air radiation.

Notice that the relative errors that will be considered in the following of this paper are consequent to the discretization of the equations, and must be distinguished from the model error that would induce a discrepancy between the simulations and physical experiments. Quantifying this discretization error allows to correctly interpret the results of simulations.

All the results are obtained with OpenWind [OpenWinD].

### 5.1 Case without dissipation

The TMM is numerically exact for the lossless model, and can therefore be taken as a reference in this case. Consequently, in order to assess the numerical quality of the FEM, we compute the relative error of the FEM solution to the reference solution obtained with the TMM,  $E_{\text{TMM}}$ , in the lossless case, defined as:

$$E_{\text{TMM}}(i) = \frac{\|Z_{i \text{ FEM}} - Z_{\text{TMM}}\|}{\|Z_{\text{TMM}}\|}, \quad (20)$$

where  $Z_{i \text{ FEM}}$  is the impedance computed using the FEM at order  $i$ , and  $Z_{\text{TMM}}$  the impedance computed using the TMM, and  $\|\cdot\|$  denotes the discrete  $\ell^2$  norm of a vector over all the considered frequencies.

The upper part of Figure 4 shows the logarithm of  $E_{\text{TMM}}(i)$  with respect to the order  $i$  of the FEM for the specific case of the trumpet bore displayed in Figure 3.

The mesh is obtained by choosing a TES equal to 3.4 cm, which gives  $N = 72$  elements, with a ratio  $\tau = 17$ . We observe that the FEM provides a solution that is closer and closer to  $Z_{\text{TMM}}$  as the order increases. After order 10 (which represents a total of 649 degrees of freedom for the  $H^1$  variable, 1369 degrees of freedom in total), the impedance relative  $\ell^2$  error does not diminish anymore and is close to  $2.6 \times 10^{-12}$ , which is dominated by roundup errors in double precision as expected. In the sequel we will call this a “converged solution”. The linear convergence in logarithmic scale agrees with the finite elements theory which predicts an exponential order (spectral) convergence. The lower part of Figure 4 shows the logarithm of  $E_{\text{TMM}}(i)$  with respect to the logarithm of the target element size (TES) of the mesh, for the different FEM orders 1 to 6. Since the trumpet bore is composed of very large and very small parts, the observed curves are not yet exhibiting asymptotic rates of convergence (we would need much smaller TES in this case). However, we observe that for a given TES (and therefore mesh), increasing the order of the FEM always diminishes the relative  $\ell^2$  error on the input impedance, achieving a precision that is difficult to reach by refining the mesh at a given order.

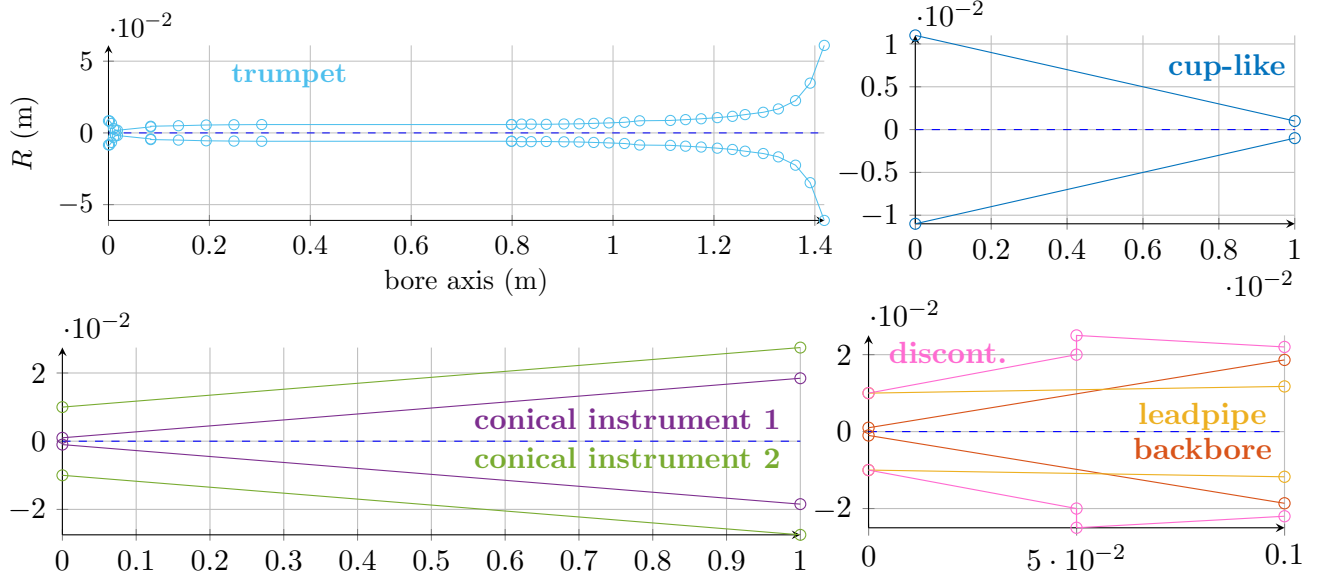


Figure 3: The seven studied bores. Top left : trumpet-like bore. Top right : simple convergent cone of general dimensions similar to a mouthpiece cup. Bottom left : two cones of 1m representative of conical instruments. Bottom right : two cones being qualitatively similar to a mouthpiece backbore and a trumpet leadpipe part, and one arbitrary geometry made of two cones, one divergent, the other convergent, and a clear discontinuity between them. The circles represent the extremities of each part. (colors online)

## 5.2 Case with dissipation

Regarding the model with viscothermal losses (lossy model), the TMM is exact for cylinders only. It will thus not be possible to use  $E_{\text{TMM}}$  to assess FEM convergence towards the exact solution for geometries of arbitrary shapes. Instead, we compute the relative  $\ell^2$  error between two finite element computations on the same mesh but consecutive orders:

$$E_{\text{order}}(i) = \frac{\|Z_{i+1}^{\text{FEM}} - Z_i^{\text{FEM}}\|}{\|Z_i^{\text{FEM}}\|}, \quad (21)$$

which is a heuristic and customary estimator when no exact solution is available (attributed to C. Runge, see [Repin(2008)]). Notice that it is not a mathematical *a posteriori* estimator [Babuska(1981), Ainsworth(1997)] but must be considered only as an illustration.

order	1	2	3	4	5+
frequential deviation (cents)	236	26	0.3	0.01	<1e-4
amplitude deviation (dB)	15	1.8	0.02	0.001	<1e-5

Table 2: Frequential position and amplitude deviations of the second impedance peak of the 20cm cylinder (radius 5mm) using the lossy model. The reference is computed using the TMM. A visual representation of this second peak is shown Figure6.

The first considered case is a cylinder 20 cm long with a 5 mm radius, which could be compared qualitatively to a trumpet leadpipe in terms of dimensions.

In Figure 5, we consider a mesh of  $N = 3$  elements and we represent both the  $E_{\text{TMM}}$  and the  $E_{\text{order}}$  relative  $\ell^2$  error estimators, since  $E_{\text{TMM}}$  is relevant in this case (it measures the distance to an exact solution). The two error estimators exhibit a very similar behavior which illustrates the fact that they are both relevant to assess the convergence of the FEM. In this case, the FEM provides a converged solution at order 9. The fact that  $E_{\text{order}}$  tends to machine precision illustrates the usual finite elements convergence theory [Fortin (1977), Cohen (2000)] which theoretically ensures that the obtained numerical solution is actually close to the exact impedance of the considered instrument (as opposed to a converged but false numerical solution) [Dauge et al.(2005)].

Figure 6 shows the modulus of the input impedance computation for the same cylinder with respect to the frequency, for different FEM orders. Table 2 gives the frequential and amplitude deviations of the second peak. The difference between the curves is visible for all orders, which is consistent with the fact that the solution is not yet converged. At a given order, the error increases with the frequency, which is known as the “pollution effect” [Gerdes and Ihlenburg(1999)]. When the order increases, the solution becomes valid in a wider frequency range. Two main effects are to be noted in the context of musical acoustics: the peaks amplitudes and frequencies can be wrong, the latter being due to numerical dispersion [Ihlenburg and Babuška(1995)]. Increasing the number of elements and/or the order allow to reduce these effects down to machine precision. In this case, at low



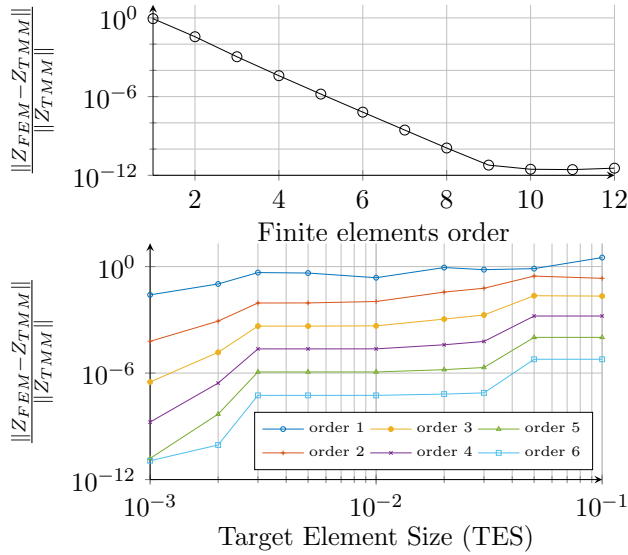


Figure 4: Relative  $\ell^2$  error between the input impedance obtained with the FEM and the TMM for the trumpet under lossless conditions. Top: the finite elements order varies on a given mesh, Bottom: the target element size (TES) varies for different FEM orders. (colors online)

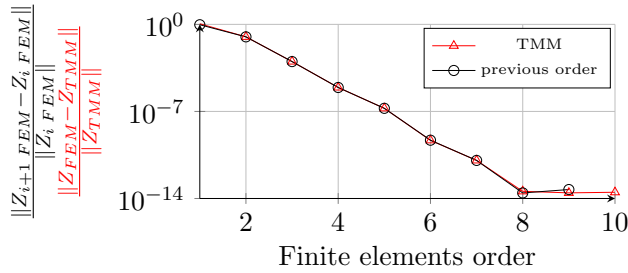


Figure 5: Comparison between  $E_{\text{order}}$  and  $E_{\text{TMM}}$  for a 20 cm cylinder of radius 5 mm using the lossy model. The FEM mesh is uniform with 3 elements.

445 orders of discretization, erroneous conclusions can be  
446 drawn if the user does not attribute the dispersion to  
447 the numerical approximation but to the model.

448 Notice finally that finite differences  
449 [Bilbao and Chick(2013)] can be seen, at least  
450 locally, as first order finite elements. The analyses of  
451 Figures 4 and 6 illustrate the fact that using a first  
452 order approximation can be a source of inaccuracy in  
453 the context of musical acoustics.

454 Figure 7 shows the logarithm of the consecutive relative  
455  $\ell^2$  error  $E_{\text{order}}$  with respect to the FEM order,  
456 considering the geometries of Figure 3, in the lossy  
457 case. The number of elements is indicated in the leg-  
458 end. An exponential order convergence is still ob-  
459 served in the presence of dissipation which is in agree-  
460 ment with the FEM theory **since only the coefficients**  
461 **have changed**. Depending on the case, the solution  
462 seems to be converged at an order ranging between 5  
463 and 10, which is related to the properties of the cho-

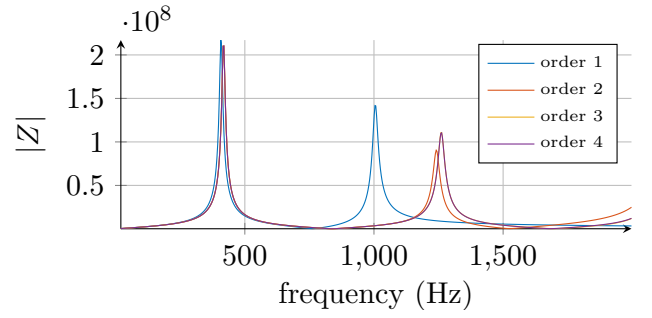


Figure 6: Modulus of the input impedance of a 20 cm cylinder of radius 5 mm computed by the FEM at different orders. (colors online)

464 sen mesh and to mathematical constants depending  
465 on the exact solution.

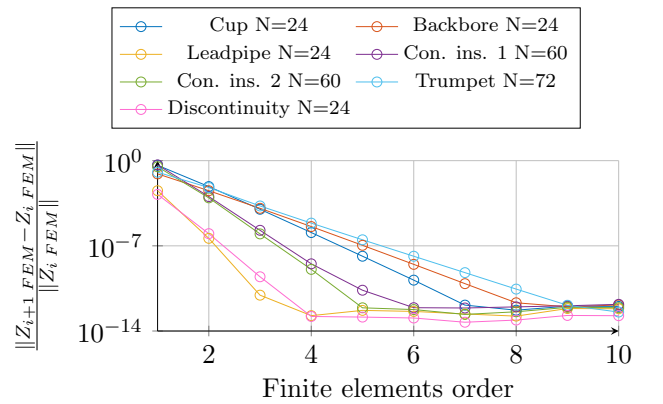


Figure 7: Consecutive relative  $\ell^2$  error between the input impedances obtained with the FEM for the lossy model using the bores of Figure 3 with respect to the FEM order. The number of elements of each mesh is given in the legend for each geometry. (colors online, matching with Figure 3)

## 6 Results

### 6.1 Study of the TMM error for arbitrary shapes considering losses

469 **Given the results of the previous sections, a converged**  
470 **FEM solution can therefore be considered as the refer-**  
471 **ence numerical solution for the lossy model, on geo-**  
472 **metries for which no exact solution is available. As**  
473 **said earlier, the TMM used on the lossy model is not**  
474 **exact for bores of arbitrary shape, and follows an em-**  
475 **pirical approach to compute input impedances, see**  
476 **section 4. In this study, we investigate the second**  
477 **empirical approach, subdividing every conical part in**  
478  **$N_{\text{sub}}$  equal segments and using for each subdivision**  
479 **the formula (17), which amounts to solving the ap-**  
480 **proximate Equations (16).**

481 It is possible to study the error made by the TMM

482 approximation, by computing the relative  $\ell^2$  error  
483 with the converged FEM input impedance:

$$E_{\text{conv FEM}}(j) = \frac{\|Z_j \text{TMM} - Z_{\text{conv FEM}}\|}{\|Z_{\text{conv FEM}}\|}, \quad (22)$$

484 where  $Z_j \text{TMM}$  is the input impedance computed using  
485 the TMM with  $j$  subdivisions for each instrument  
486 part, and  $Z_{\text{conv FEM}}$  is the converged impedance obtained  
487 by the FEM.

488 Since both methods solve different systems of equations  
489 (namely, Equations (7) for the FEM and Equations (16)  
490 for the TMM), the error between their solutions will be  
491 related to the difference between their equations [Chabassier  
492 and Tournemene(2019)]. As  $j$  increases, the TMM equations  
493 tend to the FEM equations and thus we expect both solutions  
494 to converge.

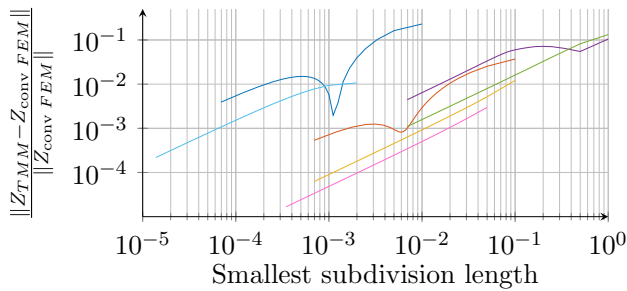


Figure 8: Relative  $\ell^2$  error between TMM solution and the converged FEM solution for the bores of Figure 3, w.r.t. the smallest subdivision length used for the TMM computation. (colors online, matching with Figure 3)

495 Figure 8 shows the logarithm of  $E_{\text{conv FEM}}$  with  
496 respect to the logarithm of the smallest subdivision  
497 length  $\Delta x_j$  used to compute  $Z_j \text{TMM}$ , for the differ-  
498 ent bores displayed in Figure 3. The relative error is  
499 computed on a frequency range of [20, 2000] Hz with a  
500 1Hz step, but the obtained results are similar when a  
501 different frequency range is considered. A first obser-  
502 vation is that all curves are decreasing at rate close to  
503 1 asymptotically (error divided by 10 when the subdivi-  
504 sions length is divided by 10). For the first conical  
505 instrument, the mouthpiece backbore and more exten-  
506 sively, for the cup-like bore, the curves show a dip  
507 for a specific subdivision length value. This can hap-  
508 pen when considering few subdivisions for each cone  
509 and disappears asymptotically, and can be interpreted  
510 as fortuitous values of  $R^\ominus$  for the cones subdivisions.  
511 More quantitatively, the error  $E_{\text{conv FEM}}$  illustrates  
512 the difference between the discretized TMM approach  
513 problem (16) and the original system (7). Because the  
514 convergence is slow (order 1 w.r.t. the subdivision  
515 length), the number of TMM subdivisions needed to  
516 obtain a solution that has converged up to machine  
517 precision is very large and induces a very heavy com-  
518 putational cost.

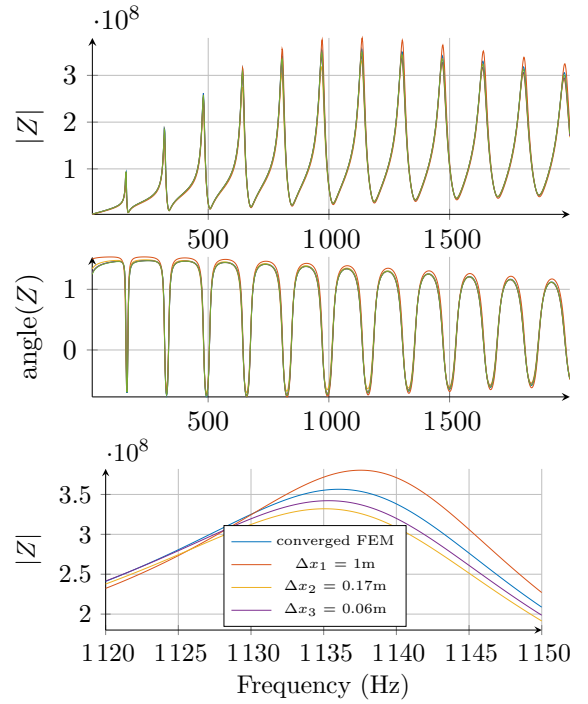


Figure 9: Impedance comparison between the converged FEM and the TMM method using different subdivision lengths of the Conical instrument 1. (colors online)

519 Figure 9 shows the input impedance of the instru-  
520 ment Conical inst. 1 on the frequency range [0, 2]  
521 kHz and [1120, 1150] Hz (close to the 7th impedance  
522 peak). On this example, the amplitude and frequency  
523 position of the impedance peaks are misjudged by the  
524 TMM when the number of subdivisions is too low.  
525 For example, the height of the 7th peak of this in-  
526 strument is 6.9% too low ( $3.56e8$  against  $3.32e8$ ) when  
527 considering a subdivision length of 0.17 m (6 subdivi-  
528 sions), and its frequency position is 1.37 cents too low  
529 (1136Hz against 1135Hz). In the case of the cup-like  
530 bore, this frequency shift is even higher (4.99 cents  
531 for the first peak around 2000Hz with a subdivision  
532 length of 0.01 m (1 subdivision) for the TMM).

## 533 6.2 Computation time and features 534 comparison of the two approaches

535 **Computation time** In the previous paragraphs,  
536 we have seen that both the FEM and the TMM are  
537 relevant to compute the input impedance of a given in-  
538 strument as defined in Equations (7). In order to com-  
539 plete the methods' performance analysis, it is neces-  
540 sary to assess and compare their computational costs.  
541 Fast input impedance computation is especially use-  
542 ful when considering optimisation applications where  
543 a large number of input impedances must be com-  
544 puted to reach optimal designs. Recall that the FEM  
545 computation requires the inversion of the sparse lin-  
546 ear system (10) while the TMM computation requires

the evaluation of the matrices product (14), both for a discrete set of pulsations  $\{\omega_i\}_{1 \leq i \leq N_\omega}$ . In the case of the FEM, most of the computation time is spent in computing the finite element matrices (10%), inverting them (39%), and evaluating the dissipative terms if any (48%) (these percentages depend somehow on the number of degrees of freedom). The matrices to invert are sparse and the overall conditioning of the matrices is good thanks to the use of spectral high order finite elements. A fair comparison can only be performed for numerical solutions that provide the same precision with respect to the exact solution. Since the FEM relies on the choice of both a mesh and an order, the same precision can be obtained with several situations that do not necessarily induce the same computational cost. In the sequel, the given time is always the smallest manually found computational time.

Firstly, for the cases where the TMM are exact (lossless case, lossy cylinder), the TMM computation is very competitive and provides the exact solution with only roundup errors. On the contrary, the FEM needs to be converged in order to provide a solution with a similar precision, and this induces an extra computational cost (about 1883 times more for the lossless trumpet and 194 times more for the lossy cylinder).

In the presence of viscothermal losses and arbitrary shapes, the TMM is not exact anymore and uses a discrete and empirical approach to compute the input impedance. We display in Figure 10 the computation times with respect to the relative  $\ell^2$  error to the converged solution, for the realistic trumpet-like bore<sup>4</sup>, for several TMM subdivision lengths (from  $\Delta x = 2\text{e-}3\text{m}$  to  $1.3\text{e-}5\text{m}$ ) and for the FEM with 35 elements at order 4.

Finally, Another FEM strategy called ‘‘adaptive’’ is also considered: it adapts the order of each mesh element to its size. This strategy avoids introducing too many degrees of freedom in small elements, improving the computation time without diminishing the global  $\ell^2$  error. In the specific case of the trumpet-like bore with a TES (Target Element Size) producing 35 elements, the first parts describing the mouthpiece are few millimeters long which is shorter than the TES. Consequently, the 4 interpolation points are unnecessarily cramped up on the only element of each of these parts. Therefore, a manual definition of the best order for each element, aided by the expected local shortest wavelength, is undertaken in order to obtain a good compromise between the number of degrees of freedom and the precision. In the example of Figure 10, the adaptive FEM improves the computation time by 11.1% compared with the usual FEM, and both computations lead to a relative  $\ell^2$  error of  $4.1 \times 10^{-4}$ .

The fastest TMM setting ( $\Delta x = 2\text{e-}3\text{m}$ ), provides a

<sup>4</sup>Computations run on a 3.4GHz Intel Core i7-2600 with 16 GB of RAM

relative  $\ell^2$  error equal to 1.1% and computes the input impedance in 0.225 seconds, which is 11.2 times faster than the adaptive FEM (2.5 seconds). The most precise TMM setting has a precision similar to the FEM ( $2.2 \times 10^{-4}$ ), but the computation time is 11.9 times higher than the adaptive FEM (30.1s). Other orders (2, 3 and 5) have been considered for the mesh of 35 elements. Corresponding results are listed in Table 3 and the order 3 is displayed on Figure 10. All the computation times are similar (between 2 and 3.2 seconds) while the errors greatly improve (from  $8.8\text{e-}2$  to  $2.5\text{e-}5$ ). This shows the overall numerical performance of the FEM in real life situations, which can target a specific precision while maintaining a competitive computation time.

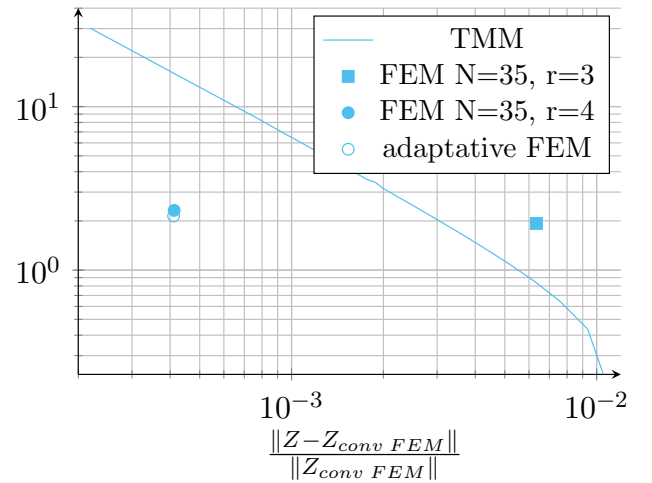


Figure 10: CPU time of the trumpet impedance computation w.r.t impedance relative  $\ell^2$  error. Comparison between the TMM and FEM methods.

elements #	35	35	35	35
order	2	3	4	5
degrees of freedom	105	140	175	210
CPU time (s)	2	2.4	2.8	3.2
$E_{\text{conv FEM}}$	$8.8\text{e-}2$	$6.3\text{e-}3$	$4.1\text{e-}4$	$2.5\text{e-}5$

Table 3: Different computation times and  $E_{\text{conv FEM}}$  considering different orders for the trumpet impedance using a 35 elements discretization.

**Acoustic variables** One immediate feature permitted by the FEM is the availability of the pressure and volume flow spectra along the entire bore axis, see Figure 11, which is directly obtained by considering all the vector  $U_h$  of system (10) (and not only the term corresponding to the input pressure). This output therefore comes at no extra computational cost compared to the impedance computation. Interpolation on arbitrary points is also possible without increasing the numerical error.

628 It could also be possible to reconstruct the pressure  
 629 and volume flow using the TMM, but it would induce  
 630 extra computational cost due to either over sampling  
 631 of the bore profile (storing intermediate results of ma-  
 632 trix products) or value interpolation (for which an ar-  
 633bitrary interpolation rule must be chosen and could  
 potentially deteriorate the numerical result).

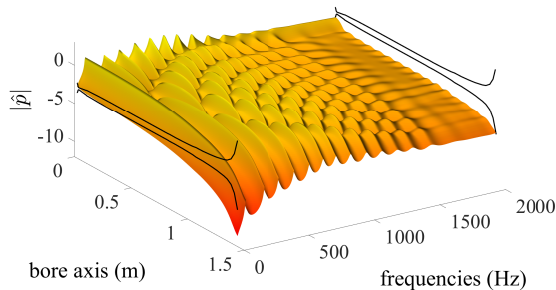


Figure 11: Evolution of the pressure modulus in logarithmic scale along the bore of the lossy trumpet according to frequency. The border at the beginning of the instrument (bore axis  $x = 0$ ) displays the input impedance. (colors online)

634 In the case of a wind instrument, it helps to under-  
 635 stand where the nodes and antinodes of the waves are  
 636 located, which may help instrument makers better vi-  
 637 sualize the instrument's functioning or even position  
 638 the toneholes<sup>5</sup>.  
 639

640 **Extended physical situations** One major advan-  
 641 tage of using FEM over TMM is the possibility to  
 642 easily solve equations with no available analytical so-  
 643 lution while maintaining an arbitrary precision. In-  
 644 deed, when more complex cases than lossless acous-  
 645 tic propagation are considered, it may be impossi-  
 646 ble to find analytical solutions, requiring the TMM  
 647 to consider some approximations if possible (visco-  
 648 thermal losses, continuously non-constant physical co-  
 649 efficients). This feature could potentially give access  
 650 to instruments impedances in very interesting phys-  
 651 ical situations. For instance, it is theoretically and  
 652 technically straightforward to consider non-constant  
 653 physical coefficients, as in the case where the temper-  
 654 ature varies inside the pipe. Indeed, this only prompts  
 655 different values for the matrices  $M_h^{L^2}$ ,  $M_h^{H^1}$ ,  $N_h^{L^2}(\omega)$   
 656 and  $N_h^{H^1}(\omega)$ . Using exactly the same quadrature for-  
 657 mulae, this only results in a different integrand taking  
 658 into account the temperature value throughout the  
 659 bore axis. The TMM can achieve a similar goal with  
 660 less flexibility and less control on the discretisation  
 661 error, refining the bore parts definition and consider-  
 662 ing a different constant temperature on each refined  
 663 parts.

<sup>5</sup>private discussion with the instrument maker Augustin Humeau

664 Table 4 shows the frequential position and ampli-  
 665 tude deviations of the 9 first impedance peaks of  
 666 the trumpet between a linear temperature gradient  
 667 [Gilbert et al.(2006)] between 37 and 21 °C, and an  
 668 averaged temperature of 29 °C inside the bore. There  
 669 is a 7% difference between the two moduli of the  
 670 impedances, showing the importance of the temper-  
 671 ature gradient for impedance calculation. More pre-  
 672 cisely, the frequential deviation varies between 0.3 and  
 673 4.2 cents (1.9 cents in average), and the peaks ampli-  
 674 tude varies between 0.1 and 0.3dB.

peak #	1	2	3	4	5	6	7	8	9
frequential deviation (cents)	4.2	1.5	1.4	1.7	2.6	1.5	1.4	2.1	0.3
amplitude deviation (dB)	0.1	0.2	0.2	0.3	0.3	0.2	0.2	0.2	0.1

Table 4: Frequential position and amplitude deviations between the two temperature profiles along the bore of the trumped for the lossy model, for the 9 first impedance peaks.

675 Other possibilities include the accurate considera-  
 676 tion of arbitrary bores (Bessel, exponential, polynomi-  
 677 als, splines, . . . ), the possible integration of new terms  
 678 in the equations or the coupling with other equations  
 679 modelling different physical phenomena (pipes junc-  
 680 tions, or excitators as lips, reeds, flue, . . . ).

## 7 Conclusion and prospects

681 The precision and performances of FEM and TMM  
 682 have been assessed, based on quantitative compari-  
 683 son, as well as the exhibition of the actual equation  
 684 solved by the TMM. In realistic cases as a trumpet  
 685 with losses, the FEM allows to compute the same  
 686 numerical solution as the TMM with a limited com-  
 687 putational cost. It also allows to compute unusual  
 688 physical situations as non-constant coefficients along  
 689 the bore. Moreover, the computation gives a direct  
 690 access to the acoustic variables inside the pipe for no  
 691 extra computational cost or over-sampling. All the  
 692 results of this article have been computed and can  
 693 be run again using the open-source python toolbox  
 694 OpenWind [OpenWInD]. Two direct extensions can  
 695 follow this work: the implementation of toneholes in  
 696 the model in order to model the input impedance of  
 697 woodwind instruments, and the sound synthesis based  
 698 on the same finite element method in space and finite  
 699 difference in time. Notice that the presence of visco-  
 700 thermal terms induces a major theoretical difficulty in  
 701 the time domain [Berjamin et al.(2017)]. Finally this  
 702 finite element framework is an efficient basis aiming at  
 703 developing an inversion algorithm based on the full-  
 704 waveform inversion [Virieux and Operto(2009)]. This  
 705 technique can be used to optimize the instrument's  
 706 geometry based on criteria derived from the input  
 707 impedance, and relies strongly on the additional out-  
 708



709 puts of the FEM impedance computation which are  
710 the pressure and flow fields inside the instrument.

## 711 References

712 [scipySparse] “[https://docs.scipy.org/doc/  
713 scipy/reference/sparse.html](https://docs.scipy.org/doc/scipy/reference/sparse.html)” .

714 [OpenWInD] “[https://gitlab.inria.fr/  
715 openwind/release](https://gitlab.inria.fr/openwind/release) under GPLv3 licence  
716 Chabassier, J., Tournemene, R.” .

717 [Ainsworth(1997)] Ainsworth, M. and Oden, J. T.  
718 (1997). “A posteriori error estimation in finite  
719 element analysis,” *Comput. Methods in Appl.  
720 Mech. Eng.* **142**, 1–88.

721 [Amestoy et al.(2000)] Amestoy, P. R., Duff, I., and  
722 L’Excellent, J.-Y. (2000). “Multifrontal par-  
723 allel distributed symmetric and unsymmetric  
724 solvers,” *Comput. Methods in Appl. Mech. Eng.*  
725 **184**, 501–520.

726 [Babuska(1981)] Babuska, I. and Dorr, M. R. (1981).  
727 “Error Estimates for the combined h and p ver-  
728 sions of the finite element method,” *Numer.  
729 Math.* **37**, 257–277.

730 [Backus(1976)] Backus, J. (1976). “Input impedance  
731 curves for the brass instruments,” *The Journal  
732 of the Acoustical Society of America* **60**(2), 470–  
733 480.

734 [Berjamin et al.(2017)] Berjamin, H., Lombard, B.,  
735 Vergez, C., and Cottanceau, E. (2017). “Time-  
736 Domain numerical modeling of brass instruments  
737 including nonlinear wave propagation, viscother-  
738 mal losses, and lips vibration,” *Acta Acust  
739 united Ac* **103**(1), 117–131.

740 [Bilbao(2009)] Bilbao, S. (2009). “Direct simulation  
741 of reed wind instruments,” *Computer Music  
742 Journal* **33**(4), 43–55.

743 [Bilbao and Chick(2013)] Bilbao, S., and Chick, J.  
744 (2013). “Finite difference time domain simula-  
745 tion for the brass instrument bore,” *J. Acoust.  
746 Soc. Am.* **134**(5), 3860–3871.

747 [Braden(2007)] Braden, A. C. P. (2007). “Bore opti-  
748 misation and impedance modelling of brass musi-  
749 cal instruments,” Ph.D. thesis, University of Ed-  
750 inburgh.

751 [Braden et al.(2009)] Braden, A. C. P., Newton,  
752 M. J., and Campbell, D. M. (2009). “Trombone  
753 bore optimization based on input impedance tar-  
754 gets,” *J. Acoust. Soc. Am.* **125**(4), 2404–2412.

755 [Brezis(2011)] Brezis, H. (2011). “Functional analy-  
756 sis, Sobolev spaces and partial differential equa-  
757 tions,” (Springer New York, London).

[Buys et al.(2017)] Buys, K., Sharp, D., and Laney,  
758 R. (2017). “Developing and evaluating a hybrid  
759 wind instrument,” *Acta Acust united Ac* **103**(5),  
760 830–846.  
761

[Campbell(2004)] Campbell, M. (2004). “Brass in-  
762 struments as we know them today,” *Acta Acust  
763 united Ac* **90**(4), 600–610.  
764

[Caussé et al.(1984)] Caussé, R., Kergomard, J., and  
765 Lurton, X. (1984). “Input impedance of brass  
766 musical instruments—comparison between exper-  
767 iment and numerical models,” *J. Acoust. Soc.  
768 Am.* **75**(1), 241–254.  
769

[Chabassier and Tournemene(2019)] Chabassier, J.,  
770 and Tournemene, R. (2019). “About the trans-  
771 fert matrix method in the context of acoustical  
772 wave propagation in wind instruments,” INRIA  
773 Research Report 9254.  
774

[Chaigne and Kergomard(2016)] Chaigne, A., and  
775 Kergomard, J. (2016). *Modern Acoustics and  
776 Signal Processing “Acoustics of Musical Instru-  
777 ments:”* (Springer New York).  
778

[Chandler-Wilde(1997)] Chandler-Wilde, S. N.  
779 (1997). “The impedance boundary value prob-  
780 lem for the Helmholtz equation in a half-plane,”  
781 *Mathematical Methods in the Applied Sciences*  
782 **20**, 813–840.  
783

[Cohen(2004)] Cohen, G. (2004). “Higher Order Nu-  
784 merical Methods for Transient Wave Equations,”  
785 (Springer, Berlin, Heidelberg).  
786

[Cohen (2000)] Cohen, G. and Fauqueux, S. (2000).  
787 “Mixed finite elements with mass-lumping for the  
788 transient wave equation,” *Journal of Computa-  
789 tional Acoustics* **8** (1), 171–188.  
790

[Courant and Hilbert(1965)] Courant, R., and  
791 Hilbert, D. (1965). “Methods of mathemat-  
792 ical physics. partial differential equations,”  
793 *Interscience* **2**.  
794

[Dalmont et al.(2001)] Dalmont, J.-P., Nederveen,  
795 C. J., and Joly, N. (2001). “Radiation impedance  
796 of tubes with different flanges: Numerical and ex-  
797 perimental investigations,” *Journal of Sound and  
798 Vibration* **244**(3), 505 – 534.  
799

[Dauge et al.(2005)] Dauge, M., Costabel, M., and  
800 Schwab, C. (2005). “Exponential convergence of  
801 hp-fem for maxwell’s equations with weighted  
802 regularization in polygonal domains,” *Math.  
803 Models Methods Appl. Sci.* **15**(4), 575–622.  
804

[Fortin (1977)] Fortin, M. (1977). “An analysis of the  
805 convergence of mixed finite element methods,”  
806 *RAIRO. Analyse Numérique* **11** (4), 341–354.  
807



- [Gerdes and Ihlenburg(1999)] Gerdes, K., and Ihlenburg, F. (1999). “On the pollution effect in FE solutions of the 3D-Helmholtz equation,” *Computer Methods in Applied Mechanics and Engineering* **170**(1–2), 155–172.
- [Gilbert et al.(2006)] Gilbert, J., Ruiz, L. L., and Gougeon, S. (2006). “Influence de la température sur la justesse d’un instrument à vent,” in *Proceedings of Congrès Français d’Acoustique 2006, Tours*.
- [Giordano(2014)] Giordano, N. (2014). “Simulation studies of a recorder in three dimensions,” *J. Acoust. Soc. Am.* **135**(2), 906–916.
- [Helie(2013)] Hélie, Thomas and Hézard, Thomas and Mignot, Rémi and Matignon, Denis (2013). “One-dimensional acoustic models of horns and comparison with measurements,” *Acta Acust united Ac* **99**(6), 960–974.
- [Ihlenburg and Babuška(1995)] Ihlenburg, F., and Babuška, I. (1995). “Dispersion analysis and error estimation of galerkin finite element methods for the Helmholtz equation,” *Int. J. Numer. Methods Engrg.* **38**, 3745–3774.
- [Kausel(2001)] Kausel, W. (2001). “Optimization of brasswind instruments and its application in bore reconstruction,” *Journal of New Music Research* **30**(1), 69–82.
- [Kirchhoff(1868)] Kirchhoff, G. (1868). “Ueber den einfluss der wärmeleitung in einem gase auf die schallbewegung,” *Annalen der Physik* **210**(6), 177–193.
- [Le Roux et al.(2008)] Le Roux, J. C., Dalmont, J.-P., and Gazengel, B. (2008). “A new impedance tube for large frequency band measurement of absorbing materials,” *J. Acoust. Soc. Am.* **123**(5), 3119.
- [Lefebvre and Scavone(2012)] Lefebvre, A., and Scavone, G. P. (2012). “Characterization of woodwind instrument toneholes with the finite element method,” *The Journal of the Acoustical Society of America* **131**(4), 3153–3163.
- [Mapes-Riordan(1993)] Mapes-Riordan, D. (1993). “Horn modeling with conical and cylindrical transmission-line elements,” *J. Audio Eng. Soc.* **41**(6), 471–484.
- [Plitnik and Strong(1979)] Plitnik, G. R., and Strong, W. J. (1979). “Numerical method for calculating input impedances of the oboe,” *The Journal of the Acoustical Society of America* **65**(3), 816–825.
- [Quarteroni et al.(2007)] Quarteroni, A., Sacco, R., and Saleri, F. (2007). “Méthodes Numériques : Algorithmes, analyse et applications,” (Springer-Verlag Mailand).
- [Rabiner and Schafer(1978)] Rabiner, L. R., and Schafer, R. W. (1978). “Digital processing of speech signals,” **100** (Prentice-hall Englewood Cliffs, NJ).
- [Repin(2008)] Repin, S. (2008). “A Posteriori Estimates for Partial Differential Equations ,”, **Radon Series on Computational and Applied Mathematics** (Berlin, Boston: De Gruyter).
- [Rienstra(2005)] Rienstra, S. W. (2005). “Webster’s horn equation revisited,” *SIAM Journal on Applied Mathematics* **65**(6), 1981–2004.
- [Sharp et al.(2011)] Sharp, D., Mamou-Mani, A., and van Walstijn, M. (2011). “A single microphone capillary-based system for measuring the complex input impedance of musical wind instruments,” *Acta Acust united Ac* **97**(5), 819–829.
- [Silva et al.(2014)] Silva, F., Vergez, C., Guillemain, P., Kergomard, J., and Debut, V. (2014). “MoReeSC: A framework for the simulation and analysis of sound production in reed and brass instruments,” *Acta Acust united Ac* **100**(1), 126–138.
- [Tournemenne et al.(2017)] Tournemenne, R., Petiot, J.-F., Talgorn, B., Kokkolaras, M., and Gilbert, J. (2017). “Brass instruments design using physics-based sound simulation models and surrogate-assisted derivative-free optimization,” *Journal of Mechanical Design* **139**(4), 041401.
- [van den Doel and Ascher(2008)] van den Doel, K., and Ascher, U. M. (2008). “Real-time numerical solution of webster’s equation on a nonuniform grid,” *IEEE Transactions on Audio, Speech, and Language Processing* **16**(6), 1163–1172, doi: 10.1109/TASL.2008.2001107.
- [Virieux and Operto(2009)] Virieux, J., and Operto, S. (2009). “An overview of full-waveform inversion in exploration geophysics,” *Geophysics* **74**(6), WCC1–WCC26.
- [Webster(1947)] Webster, J. C. (1947). “An electrical method of measuring the intonation of cup-mouthpiece instruments,” *The Journal of the Acoustical Society of America* **19**(5), 902–906.
- [Zwikker and Kosten(1949)] Zwikker, C., and Kosten, C. W. (1949). “Sound absorbing materials,” (Elsevier).